



UNIVERSITÀ DI PARMA

ARCHIVIO DELLA RICERCA

University of Parma Research Repository

Reconstructing the release history of a contaminant source with different precision via the ensemble smoother with multiple data assimilation

This is the peer reviewed version of the following article:

Original

Reconstructing the release history of a contaminant source with different precision via the ensemble smoother with multiple data assimilation / Chen, Z.; Xu, T.; Gomez-Hernandez, J. J.; Zanini, A.; Zhou, Q.. - In: JOURNAL OF CONTAMINANT HYDROLOGY. - ISSN 0169-7722. - 252:(2023), p. 104115. [10.1016/j.jconhyd.2022.104115]

Availability:

This version is available at: 11381/2936645 since: 2023-01-11T09:51:37Z

Publisher:

Published

DOI:10.1016/j.jconhyd.2022.104115

Terms of use:

Anyone can freely access the full text of works made available as "Open Access". Works made available

Publisher copyright

note finali coverpage

(Article begins on next page)

Reconstructing the release history of a contaminant source with different precision via the ensemble smoother with multiple data assimilation

Zi Chen^{a,c}, Teng Xu^{b,*}, J. Jaime Gómez-Hernández^c, Andrea Zanini^d, Quanping Zhou^a

^a*Nanjing Geological Survey Center, China Geological Survey, Nanjing, China*

^b*State Key Laboratory of Hydrology-Water Resources and Hydraulic Engineering, Hohai University, Nanjing, China*

^c*Institute of Water and Environmental Engineering, Universitat Politècnica de València, Valencia, Spain*

^d*Department of Engineering and Architecture, Università degli Studi di Parma, Parma, Italy*

Abstract

Identifying a contaminant time-varying release history is an ill-posed problem but crucial for groundwater contamination issues. A precise inversed release history offers a promising estimation of contaminant movement and is of great importance for environmental monitoring and further management. In this paper, a recent emerging data assimilation method, the ensemble smoother with multiple data assimilation (ES-MDA) is employed to handle this conundrum. The study starts with some synthetic cases in which several factors are analyzed, such as the observation data frequency, covariance inflation schemes, iteration numbers used in the ES-MDA for the purpose of identifying a time-varying contaminant injection event with different precision. The results show that the ES-MDA performs well in recovering the release history when the injection is discretized into 50 or 100-time steps but encounters fluctuation problems in the cases with 300-time steps. Further comparison reveals that the observation data frequency is a very influential factor, while the number of iterations or the kind of covariance inflation used has a lesser effect.

Keywords: Inverse modeling, Source identification, inflation factor, Data assimilation,

*Corresponding author

Email address: teng.xu@hhu.edu.cn (Teng Xu)

1. Introduction

Groundwater contamination has gained extensive attention over the last several decades (e.g., Feyen et al., 2003b; Li et al., 2011; Feyen et al., 2003a; Gómez-Hernández et al., 2003) since it is becoming a huge threat to our ecosystem. Determining the responsible for the pollution is a forensic hydrogeology task needed to ensure the accountability of those responsible. This is not an easy task, since, in general, only a few observations downstream from the source are available when the contamination is first detected. Even with the help of advanced groundwater models, and with assumptions such as knowing the release location, identifying the release history, and, therefore, the total amount of pollutants injected into the aquifer, has proven to be a complicated endeavour. A challenge that faces the problem of ill-posedness (Skaggs & Kabala, 1994; Carrera & Neuman, 1986) common to all inverse problems (Franssen & Gómez-Hernández, 2002; Capilla et al., 1998; Wen et al., 1999) . Various methods have been devised to address this problem and several reviews have been published in the subject (e.g., Atmadja & Bagtzoglou, 2001; Michalak & Kitanidis, 2004; Bagtzoglou & Atmadja, 2005; Sun et al., 2006; Gómez-Hernández & Xu, 2021).

Among all these methods, one branch, data assimilation methods, comes out ahead because of its ability to deal with huge amounts of observed data simultaneously. Data assimilation methods are versatile, efficient, and simple to understand and implement (Zhou et al., 2014). Among the data assimilation methods, the ensemble Kalman filter (EnKF) stands out. It was first proposed by Evensen (2003) in order to deal with the nonlinear relationship between parameters and state variables in inverse problems and has gained popularity in multidisciplinary fields such as oceanography, meteorology, and geology (e.g., Houtekamer & Mitchell, 2001; Bertino et al., 2003; Chen & Zhang, 2006; Aanonsen et al., 2009). Specifically, in hydrogeology, the EnKF method has proven the ability to inverse identify aquifer param-

eters, such as hydraulic conductivity (Chen & Zhang, 2006; Huang et al., 2009; Kurtz et al., 2014), porosity (Li et al., 2012), recharge rates (Franssen & Kinzelbach, 2009), boundary conditions (Chen & Zhang, 2006) and also transport-related parameters (Lan et al., 2018). More recently, researchers have started to employ EnKF variants to identify the parameters describing a contaminant source in aquifers. Butera et al. (2013) employ a geostatistical approach with some weak hypotheses to identify the pollutant release history and the source location. Xu & Gómez-Hernández (2016) use the restart normal-score Ensemble Kalman filter (Ns-EnKF) for contaminant source identification in a synthetic deterministic aquifer and later extended this method to jointly identify hydraulic conductivity and source information (Xu & Gómez-Hernández, 2018). Then, Chen et al. (2018) move one step further, to identify contaminant source information plus the position and length of a vertical barrier in a sandbox experiment via the restart Ensemble Kalman filter. Chen et al. (2018) also discuss the influence of different inflation methods in the application of the restart Ns-EnKF and prove its ability for the joint identification of hydraulic conductivities and contaminant source information in a laboratory sandbox experiment. Li et al. (2019) used Kalman filtering combined with a mixed-integer nonlinear programming optimization model to deduce the accurate location and release history of a contaminant source. The aforementioned works are a strong demonstration that the EnKF and its variants are valid methods for contaminant source identification. However, except for the work by Butera et al. (2013), the release history identified in these works only focuses on a constant pulse, the magnitude of which is independent of time.

As an alternative to the EnKF, the ensemble smoother (ES), which was first introduced by van Leeuwen & Evensen (1996), assimilates all available data in one single step instead of updating the state variable sequentially. Thus, it is expected that it should be able to identify time-varying parameters better than the EnKF (and at a cheaper price). The EnKF and the ES produce the same results when they deal with linear state-transfer functions since they

51 are based on the same covariance-based formulation (Evensen, 2004). However, in studying
52 process with strong nonlinearities, such as in the case of inverting the groundwater flow and
53 mass transport equations, the EnKF outperformed the ES (Evensen & van Leeuwen, 2000),
54 until an iterative variant of the ES was proposed, the ES with Multiple Data Assimilation
55 (ES-MDA), by Emerick & Reynolds (2013). Evensen (2018) compared the ES-MDA with
56 other iterative ensemble smoothers to solve history matching problems. Ranazzi & Sampaio
57 (2019) investigated the influence of the ensemble size on the use of an adaptive ES-MDA for
58 history matching. Todaro et al. (2019) use the ES-MDA to find a solution to the reverse flow
59 routing problem. Bao et al. (2020) coupled Generative Adversarial Networks and ES-MDA
60 methods, then use them to reconstruct the channel structures and reduce the uncertainty of
61 hydraulic head and contaminant concentration predictions. Xu et al. (2021) employed the
62 ES-MDA to identify contaminant source parameters and heterogeneous hydraulic conductiv-
63 ity jointly with the comparison with restart EnKF. Todaro et al. (2021) employed ES-MDA
64 for the simultaneous identification of the source location and the release history of a ground-
65 water contamination event. These works are all good examples of ES-MDA dealing with
66 time-varying input parameters. However, most of the aforementioned work approximated
67 the time-varying parameters by a multiple step function without analyzing the impact that
68 the step size had in the results.

69 In this work, the ES-MDA is employed to identify a time-varying release history in both
70 synthetic and real cases, the capacity of ES-MDA in identifying a release history function as
71 a function of the discretization used to approximate it is analyzed first. Then, a synthetic
72 case is studied where the influence of observation data frequency and number of ES-MDA
73 iterations are discussed. The synthetic also served to analyze two covariance inflation proce-
74 dures (e.g., Le et al., 2016; Rafiee & Reynolds, 2017) to prevent smoother collapsing. Next,
75 the ES-MDA is applied to the identification of release history functions in two sandbox ex-
76 periments. The paper is organized as follows: in section 2, we describe the methodology; in

77 section 3, the synthetic and the real sandbox experiment are presented, followed by the setup
 78 of different scenarios and evaluation criteria. Finally, in section 4, we discuss the results and
 79 draw some conclusions.

80 **2. Methodology**

81 *2.1. Groundwater flow and solute transport equations*

82 In this work, the contaminant is injected with a given flow rate into a transient ground-
 83 water flow system. Thus, the governing equations includes both the transient groundwater
 84 flow equation (Bear, 1972) and the solute transport equation (Zheng & Wang, 1999):

$$85 \quad S_s \frac{\partial h}{\partial t} = \nabla \cdot (K \nabla h) + w, \quad (1)$$

$$86 \quad \frac{\partial (\theta C)}{\partial t} = \nabla \cdot (\theta D \cdot \nabla C) - \nabla \cdot (\theta v C) - q_s C_s, \quad (2)$$

88 where, S_s represents the specific storage [L^{-1}]; h is the hydraulic head [L]; t denotes time
 89 [T]; $\nabla \cdot$ is the divergence operator, while ∇ represents the gradient operator; K denotes
 90 the hydraulic conductivity [LT^{-1}] and w represents distributed sources or sinks [T^{-1}], θ
 91 represents the porosity of the medium [-]; C is dissolved concentration [ML^{-3}]; D represents
 92 the hydrodynamic dispersion coefficient tensor [L^2T^{-1}]; v is the flow velocity vector [LT^{-1}]
 93 derived from the solution of the flow equation; q_s represents volumetric flow rate per unit
 94 volume of aquifer associated with a fluid source or sink [T^{-1}] and C_s is the concentration of
 95 the source or sink [ML^{-3}].

96 *2.2. Ensemble Smoother with Multiple Data Assimilation(ES-MDA)*

97 As we mentioned before, the ES-MDA is an improvement of the ES made by Emerick &
 98 Reynolds (2013) for handling nonlinear models. It is an iterative version of the ES where the
 99 number of iterations is predefined. The method is easy to understand and to implement and

100 has been referred many times in the literature (Emerick & Reynolds, 2013; Evensen, 2018;
101 Xu et al., 2021). A brief recall of the three steps that conform the method are described
102 next.

103 1. Initialization step.

104 An ensemble of N_e realizations of the n parameters to identify is generated. In this
105 case, the parameters are the mass loadings in time representing the discretized injection
106 curve; their initial values are drawn from predefined uniform distributions. (Each ensemble
107 member is a different release history function.) At this stage, we also need to set the number
108 of iterations N_a (also referred to as assimilation steps), and the inflation factors α_j ; the
109 meaning of which are described later.

110 2. Assimilation.

111 Once the number of iterations and the inflation coefficients are determined, it is time for
112 the assimilation procedure, which consists of two steps, a forecast step, and an update step.
113 These two steps are repeated for each iteration.

114 a. Forecast step

115 In this step, the groundwater flow and contaminant transport models, MODFLOW (Mc-
116 Donald & Harbaugh, 1988) and MT3DS (e.g., Zheng, 2010; Ma et al., 2012), are run for each
117 member of the ensemble; in our case, for each different release history,

118
$$C_{i,j}^f = \psi[C_0, A_{i,j}], \quad (3)$$

119 where ψ represents the forward numerical model, $C_{i,j}^f$ are the predicted concentrations (in
120 space and time) at assimilation iteration j for the last estimate of the release function i of
121 the ensemble, $A_{i,j}$. The size of A depends on the number of time steps used to discretize it.

122 b. Update step

123 Then, the model parameters are updated as follows,

$$124 \quad A_{i,j+1} = A_{i,j} + \Delta A_j (\Delta C_j^f)^T [\Delta C_j^f (\Delta C_j^f)^T + \alpha_j R]^{-1} [y_{obs} + \sqrt{\alpha_j} \varepsilon - C_{o,i,j}^f], \quad (4)$$

125 where y_{obs} is a column vector with dimensions $N_o \cdot N_t$ containing all observed concentrations
 126 at all locations and all time steps (N_o is the number of locations, and N_t the number of
 127 observation steps); ε stands for the observation error, while R is the covariance matrix of the
 128 observation error; $C_{o,i,j}^f$ is the vector of forecasted concentrations for the ensemble parameter
 129 set $A_{i,j}$ at the same locations and times where and when observations y_{obs} are made; ΔA_j
 130 and ΔC_j are matrices defined as

$$131 \quad \Delta A_j = \frac{1}{\sqrt{N_e - 1}} [A_{1,j} - \bar{A}_j, A_{2,j} - \bar{A}_j, \dots, A_{N_e,j} - \bar{A}_j], \quad (5)$$

$$132 \quad \Delta C_j^f = \frac{1}{\sqrt{N_e - 1}} [C_{1,j}^f - \bar{C}_j^f, C_{2,j}^f - \bar{C}_j^f, \dots, C_{N_e,j}^f - \bar{C}_j^f], \quad (6)$$

134 where \bar{A}_j and \bar{C}_j^f are the ensemble means of source release history parameters and forecasted
 135 concentrations at the j th iteration, respectively. The products $\Delta C_j^f (\Delta C_j^f)^T$ and $\Delta A_j (\Delta C_j^f)^T$
 136 are the concentration covariance and the concentration-release function parameters cross-
 137 covariance, respectively.

138 These forecast and update steps will be repeated until the predefined iterations are com-
 139 pleted. One more thing needs to be pointed out: in our study, since the number of mea-
 140 surements is larger than the ensemble size, it is necessary to employ the truncated singular
 141 value decomposition (TSVD) method to compute a pseudo-inverse in Eq. (4).

142 2.3. The inflation factors α_j

143 The iteration number (N_a) and the inflation factor (α_j) are two influential parameters
 144 in the performance of the ES-MDA, which are related to one another. Emerick & Reynolds
 145 (2013) have proven that the ES-MDA could sample the posterior probability distribution

146 function of the parameters precisely only in a linear model and only if the inflation factors
 147 α_j satisfy the following equation,

$$148 \quad \sum_{j=1}^{N_a} \frac{1}{\alpha_j} = 1, \quad (7)$$

149 There are still many options on how to choose the α_j parameters satisfying the previous
 150 equation. Apparently, choosing a decreasing series may be the most appropriate, but some
 151 authors claim that using uniform values gives similar results, and that choosing these values
 152 arbitrarily may lead to filter collapse (Le et al., 2016). We have decided to explore two
 153 methods to select the inflation factors, one proposed by Rafiee & Reynolds (2017), and the
 154 other one proposed by Evensen (2018).

155 Rafiee & Reynolds (2017) propose that the inflation factor for the first iteration is com-
 156 puted as

$$157 \quad \alpha_1 = \left(\frac{1}{N} \sum_{i=1}^N \lambda_i \right)^2, \quad (8)$$

158 where N is the minimum of N_e and $N_o \cdot N_t$, and λ_i are the singular values of matrix D_j given
 159 by

$$160 \quad D_j = R^{-\frac{1}{2}} \Delta C_j^f. \quad (9)$$

161 The subsequent inflation factors are chosen in a geometrical decreasing progression,

$$162 \quad \alpha_j = \beta^{j-1} \alpha_1, \quad (10)$$

163 where β is the ratio that fulfills that the sum of the inverse of the inflation factors equals
 164 one (Eq. (7))

$$165 \quad \frac{1 - (1/\beta)^{N_a-1}}{1 - 1/\beta} = \alpha_1. \quad (11)$$

166 Evensen (2018) define the inflation factors on the basis of two numbers, a nonzero value
 167 α'_1 and a geometrical ratio α_{geo} ; with these two numbers, a sequence is built according to

168 the following procedure

$$169 \quad \alpha'_{j+1} = \frac{\alpha'_j}{\alpha_{geo}}, \quad (12)$$

170 which is then normalized to provide the α_j values that satisfy Eq. (7)

$$171 \quad \alpha_j = \alpha'_j \left(\sum_{j=1}^{N_a} \frac{1}{\alpha'_j} \right) \quad (13)$$

172 This scheme has the capacity of defining the inflation factors as uniform, in an increasing
173 sequence or in a decreasing one by choosing an α_{geo} equal, below or above one, respectively.
174 Here, we define α_{geo} and α'_1 with the values of 2 and 1, respectively.

175 In this work, these two different schemes of generating the inflation factors are employed,
176 and their impact is discussed.

177 **3. Applications**

178 A numerical model based on real sandbox experiments is used to demonstrate the pro-
179 posed method. This sandbox equipment was built up by the Engineering and Architecture
180 Department at the University of Parma, and has been employed in several groundwater con-
181 tamination studies (Citarella et al., 2015; Cupola et al., 2015; Zanini & Woodbury, 2016). In
182 this work, first, we generated synthetic data using this numerical model to test the ES-MDA
183 method for the identification of a time-varying release history curve. In the synthetic case,
184 we also analyze the impact of the choice of the method to choose the inflation factors, the
185 number of iterations, the size of the observation time intervals, and the degree of discretiza-
186 tion with which the release curve is represented in the numerical model. Then, we tested
187 the ES-MDA with real observation data and analyzed the impact of the observation error
188 magnitude.

189 *3.1. Sandbox Set-up*

190 The sandbox has an internal volume of 95 cm by 10 cm by 70 cm and is discretized
 191 into 95 columns, 1 row, and 70 layers. The reference hydraulic field inside the sandbox
 192 is shown in Figure 1. The reservoirs upstream and downstream are set up as constant
 193 piezometric boundaries with a water level of 62.5 cm and 60.6 cm, respectively. The bottom
 194 of the sandbox is regarded as a no-flow boundary while the top of the sandbox is a phreatic
 195 surface. An injector was installed inside the glass beads that discharges fluorescein during
 196 the experiment. Contaminant concentrations are observed in 25 observation points. The
 197 details about the acquisition of the concentration data could be found in Citarella et al.
 198 (2015); Cupola et al. (2015). The total experiment time is 3000 s and the injection starts at
 199 time zero. The main hydraulic parameters used for the simulation are listed in Table 1.

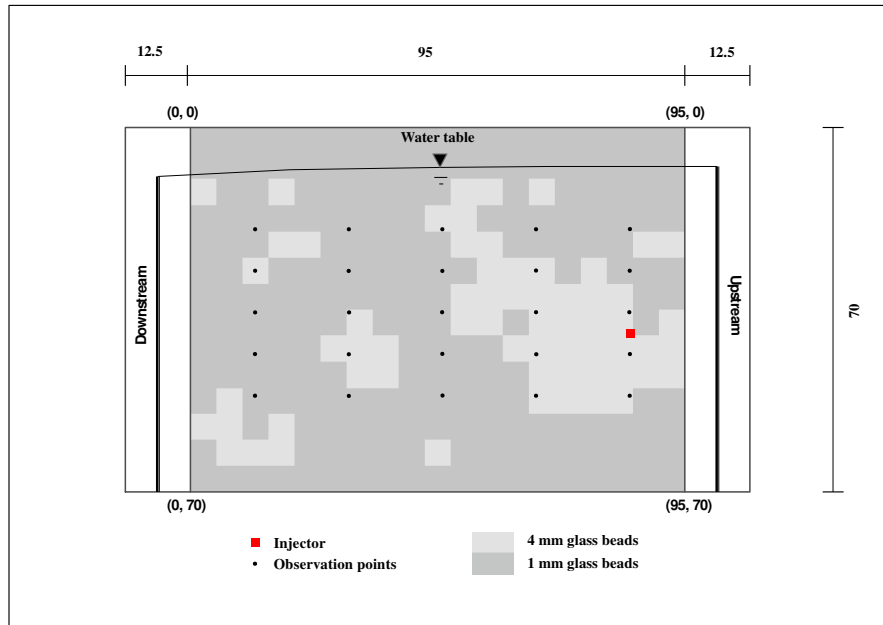


Figure 1: Sketch of the experimental device (lateral view). Length unit is cm.

Table 1: Parameters of the groundwater flow and transport models

	1 mm glass beads	4 mm glass beads
Hydraulic conductivity (cm/s)	0.65	10.4
Longitudinal dispersivity, α_T (cm)	0.106	0.2
Porosity	0.37	0.37
TRVT, α_T/α_L	0.45	0.45

200 *3.2. Performance Assessment*

201 The use of an ensemble-based method allows to analyze the performance of the method
 202 using the root mean square error (RMSE) and the relative RMSE:

$$203 \quad RMSE = \sqrt{\frac{1}{n} \sum_{i=1}^n (A^{ref} - \bar{A}_i)^2}, \quad (14)$$

$$204 \quad \text{relative } RMSE = \frac{RMSE}{\text{initial } RMSE}, \quad (15)$$

205 where n is the number of points used to discretize the release history curve, A^{ref} is the
 206 reference release history while \bar{A} stands for the ensemble mean of the updated release history,
 207 initial $RMSE$ refers to the $RMSE$ of the initial ensemble of realizations.

208 Based on the definition of RMSE, the smaller the value, the better. The relative RMSE
 209 is able to show the reduction of the uncertainty. Both parameters serve to evaluate quanti-
 210 tatively the outcome of ES-MDA.

211 *3.3. Synthetic Case*

212 The first set of analyses is based on the synthetic simulation of a time-varying release
 213 into the sandbox digital twin. The release function adopted is based on a proposal by Skaggs

214 & Kabala (1994):

$$\begin{aligned} S(t) = & 2.6 \cdot \exp\left(-\frac{\left(\frac{t}{10} - 20\right)^2}{50}\right) \\ & + 0.78 \cdot \exp\left(-\frac{\left(\frac{t}{10} - 50\right)^2}{200}\right) \\ & + 1.3 \cdot \exp\left(-\frac{\left(\frac{t}{10} - 90\right)^2}{98}\right) \quad 0 \leq t \leq 3000. \end{aligned} \quad (16)$$

216 This function is shown in Figure 2. We run three sets of scenarios with different time
217 discretizations while identifying the release history. More precisely, we chose to identify a
218 release function over the 3000 s experiment duration using 50, 100, and 300 time steps. For
219 each discretization, two sampling frequencies were considered: samples were taken every
220 other time step or every ten time steps. Also, the number of assimilation iterations was
221 varied between 4 and 8, and both the Rafiee and Evensen inflation schemes were tested. In
222 total 24 scenarios were analyzed as reported in Table 2. And in all scenarios, the model
223 error is neglected while we assume the observation errors follow Gaussian distribution with
224 a mean of 0 and standard deviation of 0.1 mg/l.

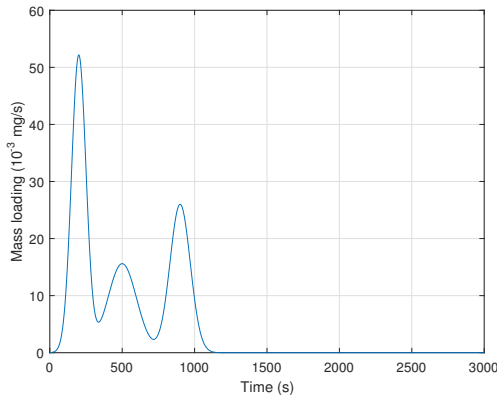


Figure 2: Release curve of a synthetic contaminant source.

225 An ensemble of 500 realizations was used. The initial release history curve of every
226 realization is generated using a uniform distribution with ranges $[0, 52] 10^{-3}$ mg/l.

227 Figure 3 shows the recovered release history for the set of scenarios with the coarsest
228 discretization of the release function: 50 time steps. In each plot, the blue curve corresponds

Table 2: Definition of the synthetic scenarios

Scenario	Number of discr. time steps	Number of time observations	Number of iterations	Inflation factor
S1	50	5	4	Rafiee's scheme
S2	50	5	4	Evensen's scheme
S3	50	5	8	Rafiee's scheme
S4	50	5	8	Evensen's scheme
S5	50	25	4	Rafiee's scheme
S6	50	25	4	Evensen's scheme
S7	50	25	8	Rafiee's scheme
S8	50	25	8	Evensen's scheme
S9	100	10	4	Rafiee's scheme
S10	100	10	4	Evensen's scheme
S11	100	10	8	Rafiee's scheme
S12	100	10	8	Evensen's scheme
S13	100	50	4	Rafiee's scheme
S14	100	50	4	Evensen's scheme
S15	100	50	8	Rafiee's scheme
S16	100	50	8	Evensen's scheme
S17	300	30	4	Rafiee's scheme
S18	300	30	4	Evensen's scheme
S19	300	30	8	Rafiee's scheme
S20	300	30	8	Evensen's scheme
S21	300	150	4	Rafiee's scheme
S22	300	150	4	Evensen's scheme
S23	300	150	8	Rafiee's scheme
S24	300	150	8	Evensen's scheme

229 to the actual release history, the gray lines are the recovered release history curves for all
230 500 realizations, the red dotted line is the median of the ensemble and the black dashed lines
231 mark the 5 and 95 percentiles. The first column uses Rafiee’s inflation and the second column
232 Evensen’s inflation. The first two rows use samples every ten time steps (5 snapshots), and
233 the last two rows samples every other time step (25 snapshots). The first and third rows
234 use four iterations and the second and fourth rows use eight iterations. It can be observed
235 that the median of the recovered release history curves is a good estimate of the actual
236 release history for almost all cases (scenarios S2 and S4 being the exception), while the
237 uncertainty estimate given by the spread of the curves is larger for the scenarios with the
238 smallest sampling frequency (scenarios S1 to S4). Also, it can be noticed that Rafiee’s
239 inflation method always yields a smaller spread than Evensen’s one. It is hard to argue
240 about an improvement with the largest number of iterations since the results with four and
241 eight iterations are almost the same.

242 Figure 4 shows the recovered release history of the set of scenarios with intermediate
243 discretization of the release function: 100 time steps. The organization of the plots in the
244 figure is the same as in the previous one. The impact of the inflation scheme, the observation
245 data frequency, and the number of iterations is more or less the same as for the 50-time step
246 case. However, the median of the recovered release history curves cannot capture the actual
247 release history as precisely as in the previous set of realizations, more notably in the set of
248 scenarios with samples every 10 time steps (scenarios S9 to S12). For all scenarios, there is
249 clearly an excess of fluctuations in the recovered release curves, noticeable in the individual
250 curves and also in the ensemble median and percentile curves. This fluctuation is more
251 noticeable when the observation sampling frequency is smaller (scenarios S9 to S12). The
252 fluctuations must be due to the inherent ill-posedness of the problem since we are trying
253 to estimate a large number of parameters that, initially, are assumed to be independent.
254 This problem could be alleviated by introducing some smoothing factor that forces that all

255 updated curves after updating display a certain smoothness. It is also important to notice
256 the poor estimation of the release curve at the end of the experiment, with a clear non-zero
257 estimation for the final steps. This overestimation, which is less patent in the previous set
258 of scenarios, must be due to the little or no sensitivity that observations have to release at
259 the end of the simulation.

260 The deterioration in the estimation of the release curves becomes exacerbated when the
261 number of discretization steps is increased up to 300. Figure 5 shows the results for scenarios
262 S17 to S24, and their arrangement follows the same pattern as the previous two figures. The
263 original release curves are only hinted at by the final ensemble of realizations or their median
264 values, the main three peaks are well identified, but several other peaks appear, the spread
265 of the realizations is very wide and the fluctuations in time are also quite noticeable. As in
266 the previous set of scenarios, using a different parameterization of the release curve enforcing
267 some kind of regularization might have helped in removing these artifacts. The only positive
268 conclusion from this set of realizations is that, as in the previous two sets, the best results
269 are always obtained when using Rafiee’s inflation scheme, eight iterations, and the highest
270 sampling frequency.

271 For a more quantitative evaluation of the performance of the ES-MDA to recover the
272 time-varying release history, Table 3 and Figure 6 illustrates the RMSE and the relative
273 RMSE of all 24 scenarios. Based on the RMSE at the last iteration step, we can conclude
274 that the ES-MDA with Rafiee’s scheme has a better performance in most scenarios for our
275 case, especially when the observation data frequency is low. It is striking to see how the
276 RMSE jumps to up to four times the RMSE of the initial ensemble on the first iteration for
277 the fine discretization scenarios (last row of Figure 6), a distinct mark of ill-posedness in the
278 formulation of the problem.

279 Based on this analysis, we decide to apply the ES-MDA to the sandbox experiment using
280 Rafiee’s inflation scheme, discretizing the release history into 50 or 100 time steps, and with

Table 3: RMSE of the synthetic scenarios at the last iteration step

Scenario	RMSE	Scenario	RMSE	Scenario	RMSE
S1	2.295	S9	3.621	S17	12.585
S2	2.136	S10	5.057	S18	15.181
S3	1.979	S11	4.222	S19	8.839
S4	1.818	S12	5.671	S20	12.103
S5	1.120	S13	1.711	S21	9.221
S6	1.178	S14	2.475	S22	8.963
S7	1.321	S15	1.891	S23	7.321
S8	1.182	S16	1.959	S24	6.853

Table 4: Definition of the sandbox scenarios for the train of pulses

Scenario	Number of discr. steps	Number of observ. time steps
R1	50	5
R2	50	25
R3	100	10
R4	100	50

281 8 assimilation iterations.

282 3.4. Laboratory Case

283 We performed two sandbox experiments with two release history curves. The first curve
 284 displays a train of four pulses lasting the entire duration of the experiment and the second
 285 curve consists of two pulses at the beginning of the experiment (Figure 7). In this experiment,
 286 we will not attempt to identify simultaneously the release and the conductivities, but rather,
 287 we will use the identified distribution of conductivities and observation errors from a previous
 288 work (Chen et al., 2021) shown in Figure 8. The observation errors follow a Gaussian
 289 distribution with zero mean and a standard deviation of 1 mg/l. Several scenarios will be
 290 analyzed that are described in Tables 4 and 4.

291 Figure 9 shows the recovered release history curves for the first sandbox experiment,
 292 the train of pulses. The observed performance is quite similar to the one observed for the
 293 synthetic experiments; the scenario with the smaller number of discretization steps and the

Table 5: Definition of the sandbox scenarios for the two pulses

Scenario	Number of discr. steps	Number of observ. time steps
R5	50	5
R6	50	25
R7	100	10
R8	100	50

294 highest frequency for that discretization is the one performing best. The same fluctuation
 295 as in the synthetic cases is observed about the four peaks of the release curve and the same
 296 uncertainty spread, which is smaller for scenario R2. Looking closer to this scenario, we can
 297 notice that the identification of the four pulses has a shift in time of a couple of time steps
 298 as if the injection had started a little bit later than in reality.

299 Figure 10 shows the recovered release curves for the second experiment, the two pulses.
 300 The same behavior as before is appreciated here. Large fluctuations about the two main
 301 peaks of the injection, with the best estimation by the median of the scenario with the
 302 smallest number of discretization steps and the largest frequency of observation for that
 303 discretization. Yet, there is a major failure in this test case in that the method is not able
 304 to capture the fact that the injection stops slightly before the middle of the experiment (at
 305 about 1200 s). In all scenarios, most injection curves for the individual members of the
 306 ensemble display positive values, and their median is still a relatively large positive value
 307 for the second half of the experiment, clearly overestimating the total mass injected into the
 308 system. The increase of values towards the end of the experiment is also quite noticeable. The
 309 main explanation for this overall behavior is the magnitude of the concentration observation
 310 error variance.

311 Table 6 and Figure 11 show the evolution of the RMSE and relative RMSE for the two
 312 sandbox scenarios. The results prove that the ES-MDA with Raffee's inflation scheme is an
 313 effective method in recovering releasing history in both sandbox experiments. The RMSE for
 314 all 8 scenarios is reduced after assimilating the observation data. A comparison among the

Table 6: The RMSE of sandbox scenarios at final iteration step

Scenario	RMSE	Scenario	RMSE
R1	24.073	R5	18.706
R2	22.419	R6	18.289
R3	24.318	R7	19.123
R4	24.878	R8	20.461

315 different sandbox scenarios also shows that a high observation data frequency has a lesser
 316 impact on the outcome than in the synthetic cases. This observation is particularly obvious
 317 for scenarios R3, R4, and R7, R8, which are the cases with 100 time steps; we believe it is
 318 mainly caused by the uncertainty about the observation data.

319 For a further evaluation of the results, we use the updated release history to generate
 320 contaminant plume evolution to visually analyze the capacity of the ES-DMA with Raffee’s
 321 inflation scheme to reproduce the real plumes. Figure 12 and Figure 13 show the ensemble
 322 means of the contaminant plumes at time steps 600 s, 1200 s, 1800 s, and 2400 s for scenarios
 323 R2, R4, R6 and R8. We can observe that the simulated plume always spreads more than
 324 the reference, a consequence of the overestimation of the non-injection period. However,
 325 compared with the reference contaminant plume in the left column, the simulated plumes
 326 from the updated release history for the 4 scenarios are all acceptable reproductions of the
 327 reference.

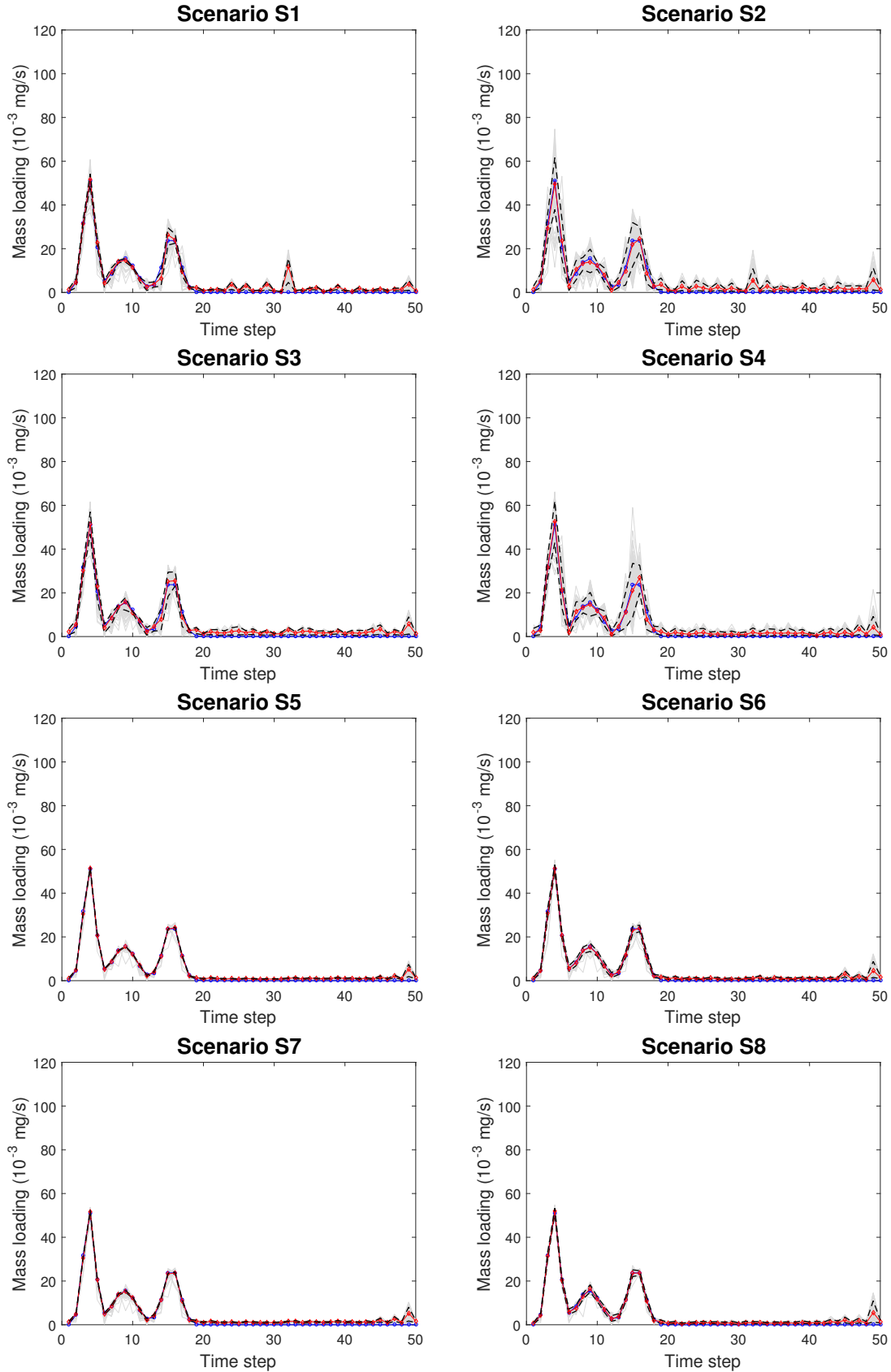


Figure 3: Recovered release histories for scenarios S1 to S8. The blue curve corresponds to the actual release history. The gray lines are the recovered release history curves for all 500 realizations, the red dotted lines is the median, and black dashed lines the 5 and 95 percentiles.

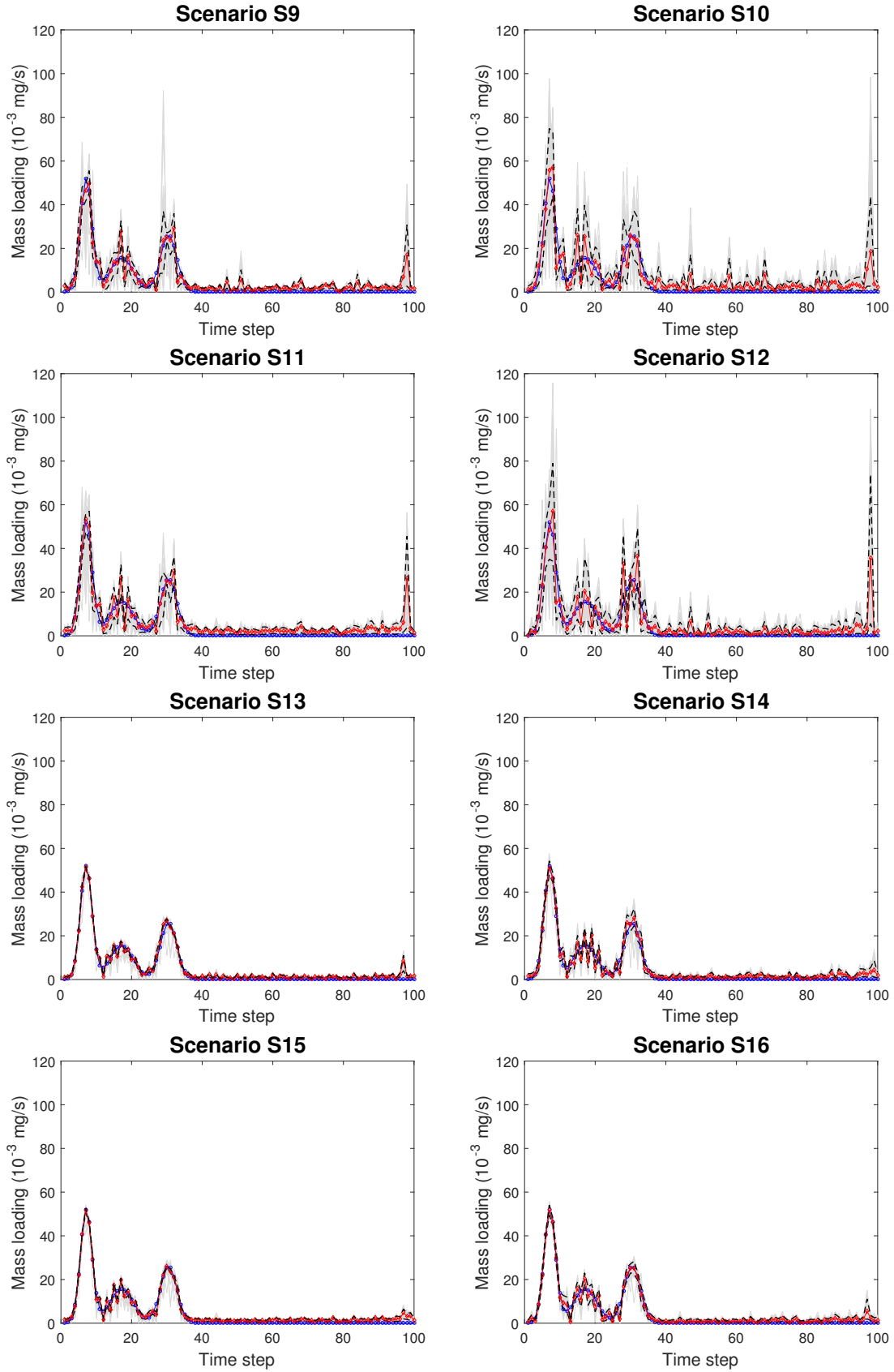
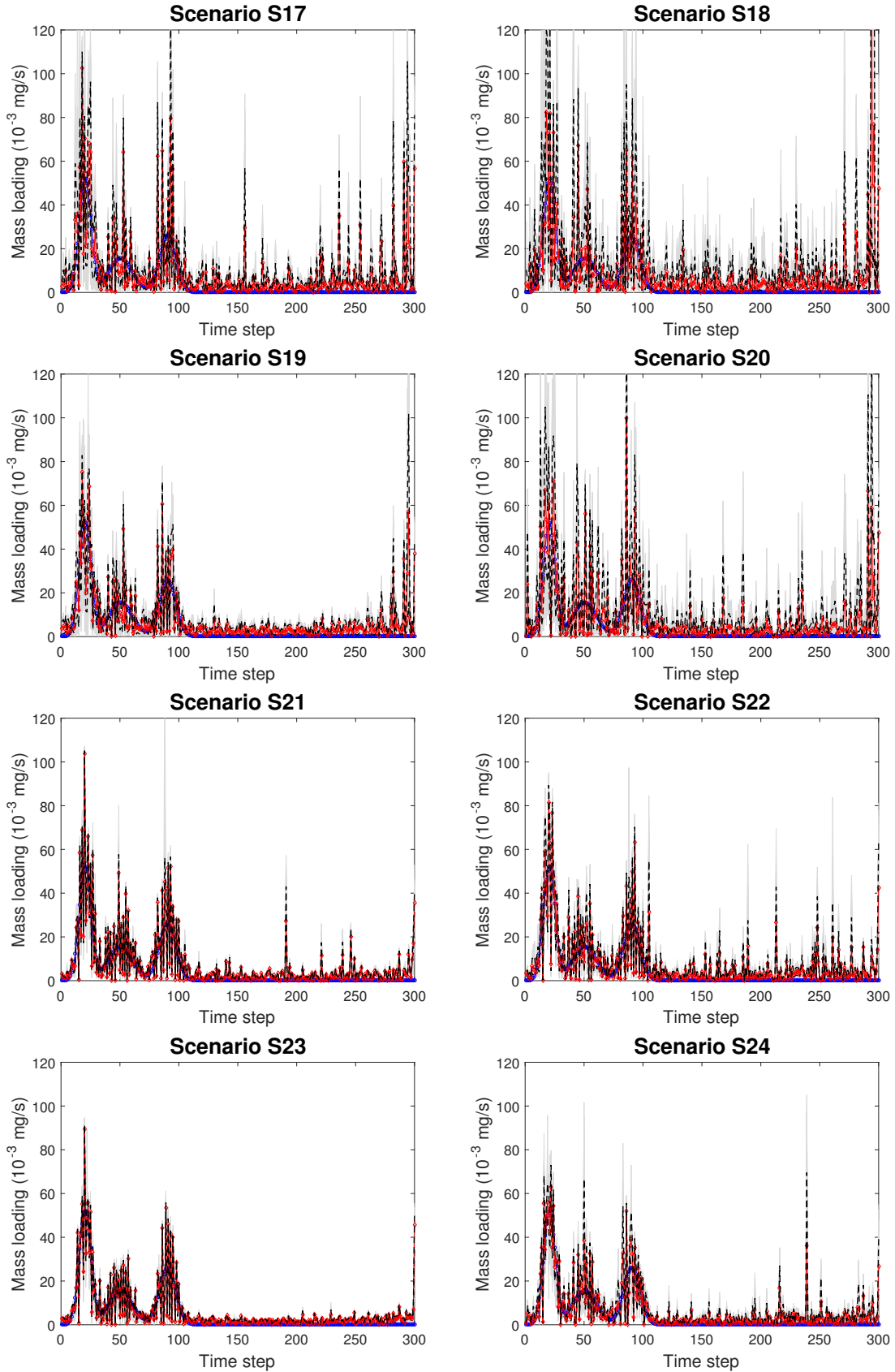


Figure 4: Recovered release histories for scenarios S9 to S16. The blue curve corresponds to the actual release history. The gray lines are the recovered release history curves for all 500 realizations, the red dotted lines is the median, and black dashed lines the 5 and 95 percentiles.



21
 Figure 5: Recovered release histories for scenarios S9 to S16. The blue curve corresponds to the actual release history. The gray lines are the recovered release history curves for all 500 realizations, the red dotted lines is the median, and black dashed lines the 5 and 95 percentiles.

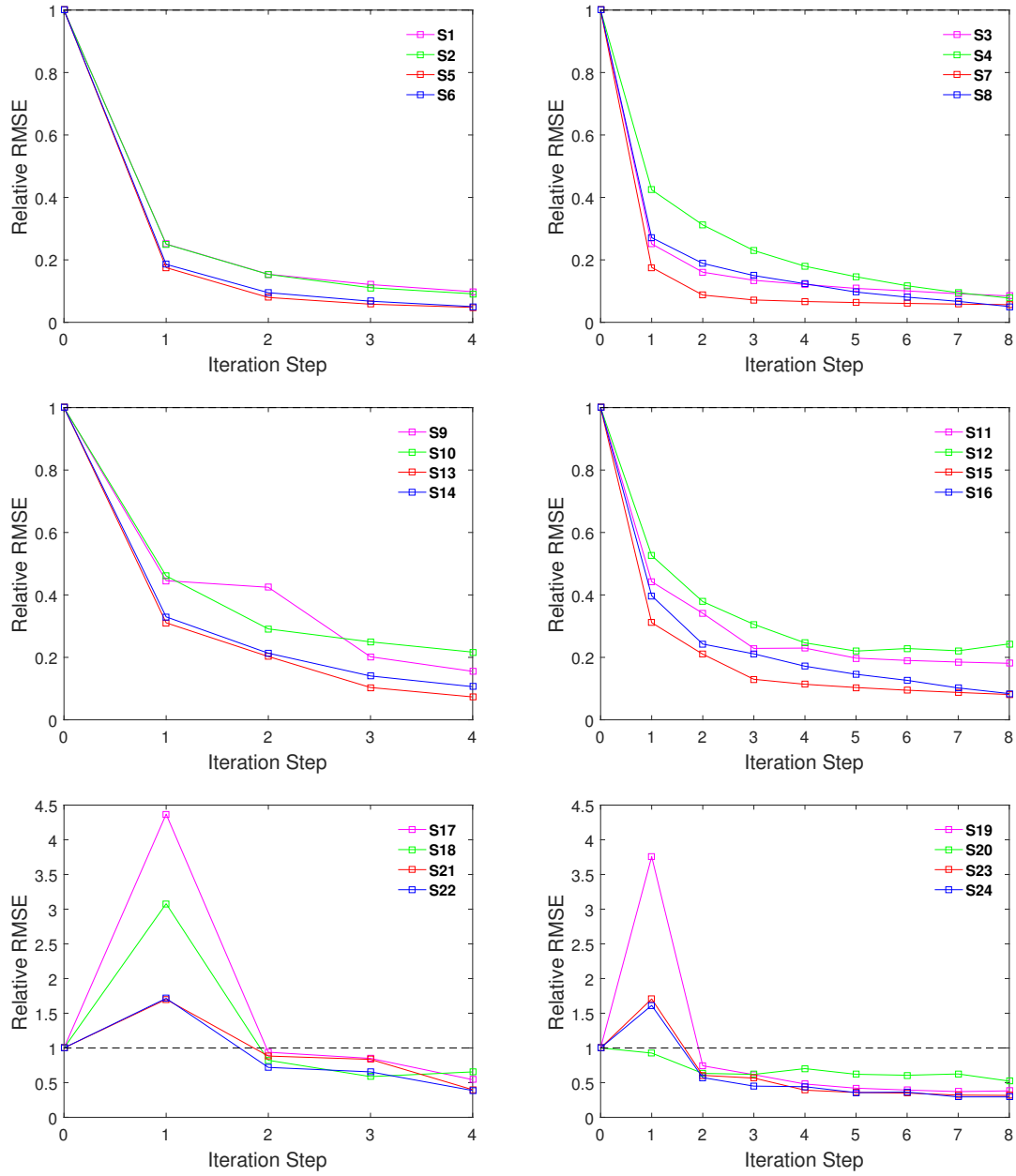


Figure 6: Evolution of the Relative RMSE for the synthetic scenarios as a function of the iteration step.

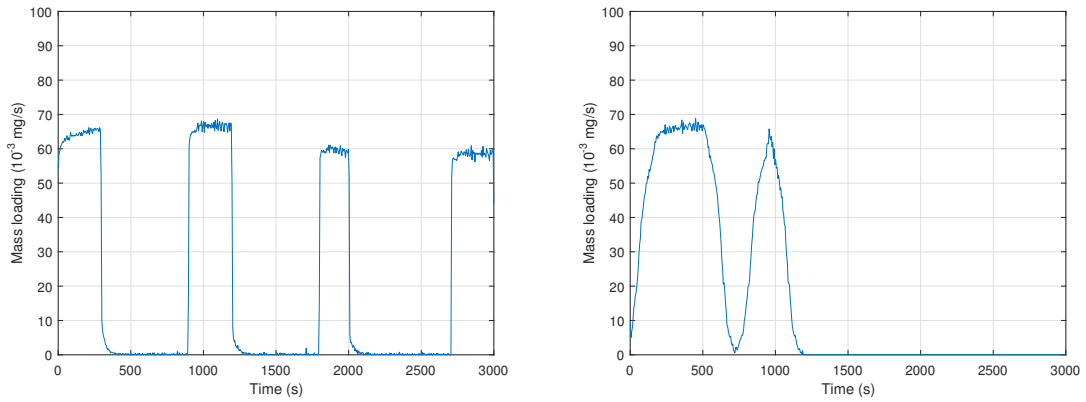


Figure 7: Release history curves for the two sandbox experiment.

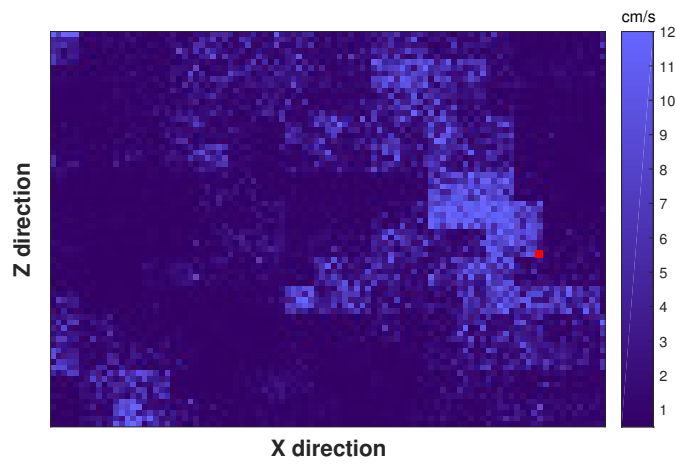


Figure 8: Hydraulic conductivity field. The red square denotes the source location. Flow and transport are from right to left.

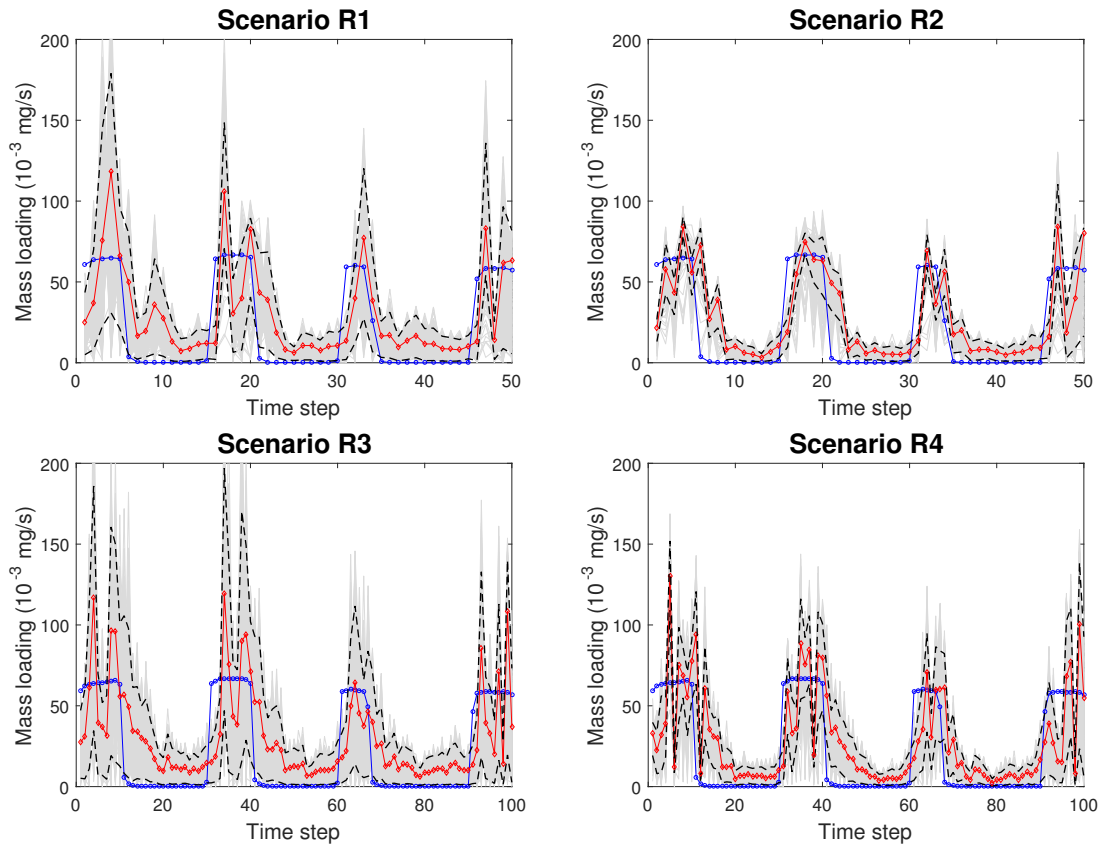


Figure 9: Recovered release history for first sandbox experiment, scenarios R1 to R4. The blue curve corresponds to the actual release history. The gray lines are the recovered release history curves for all 500 realizations, the red dotted lines is the median, and black dashed lines the 5 and 95 percentiles.

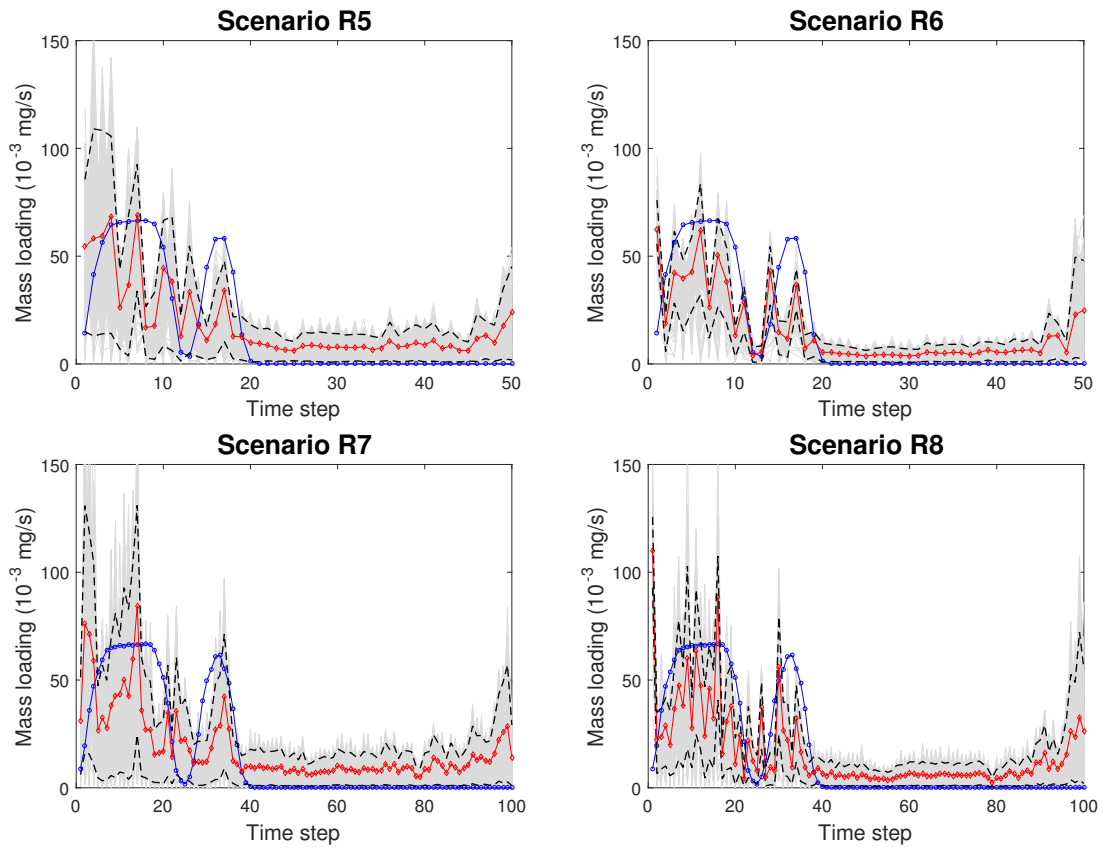


Figure 10: Recovered release history for the second sandbox experiment, scenarios R5 to R8. The blue curve corresponds to the actual release history. The gray lines are the recovered release history curves for all 500 realizations, the red dotted lines is the median, and black dashed lines the 5 and 95 percentiles.

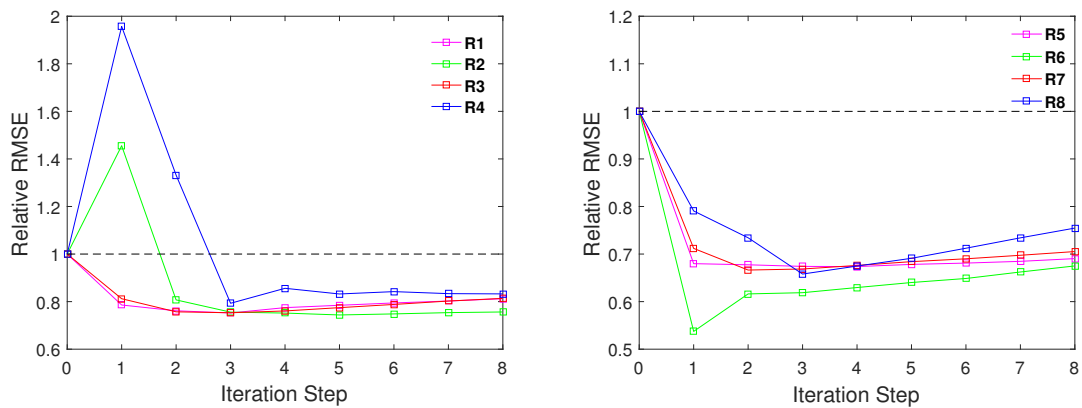


Figure 11: Relative RMSE of sandbox scenarios(R1-R8)

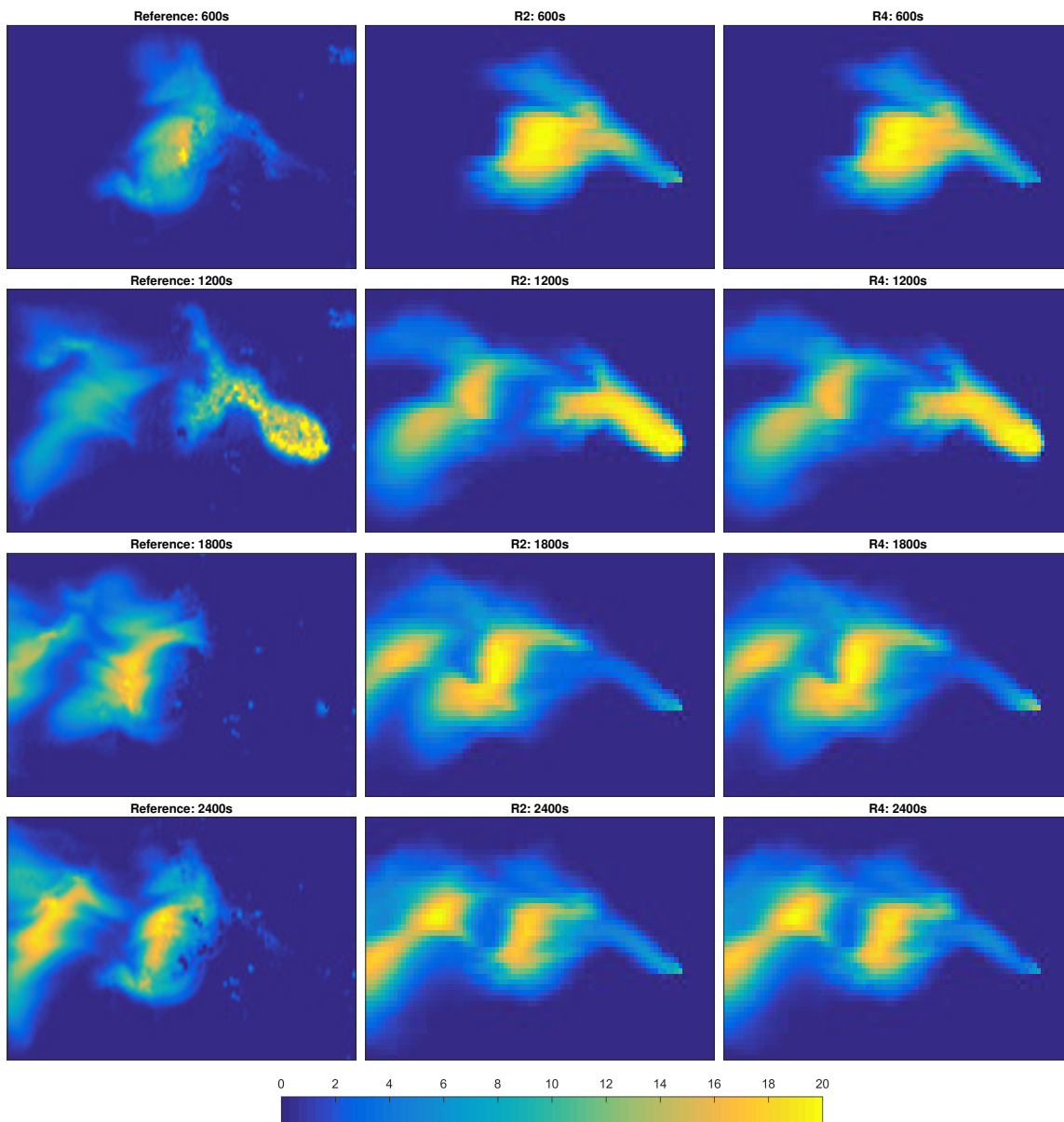


Figure 12: First sandbox experiment: train of pulses. Ensemble mean of the contaminant plume evolution obtained with the updated release functions for scenarios R2 and R4 at 600 s, 1200 s, 1800 s and 2400 s. The first column corresponds to the reference contaminant plume.

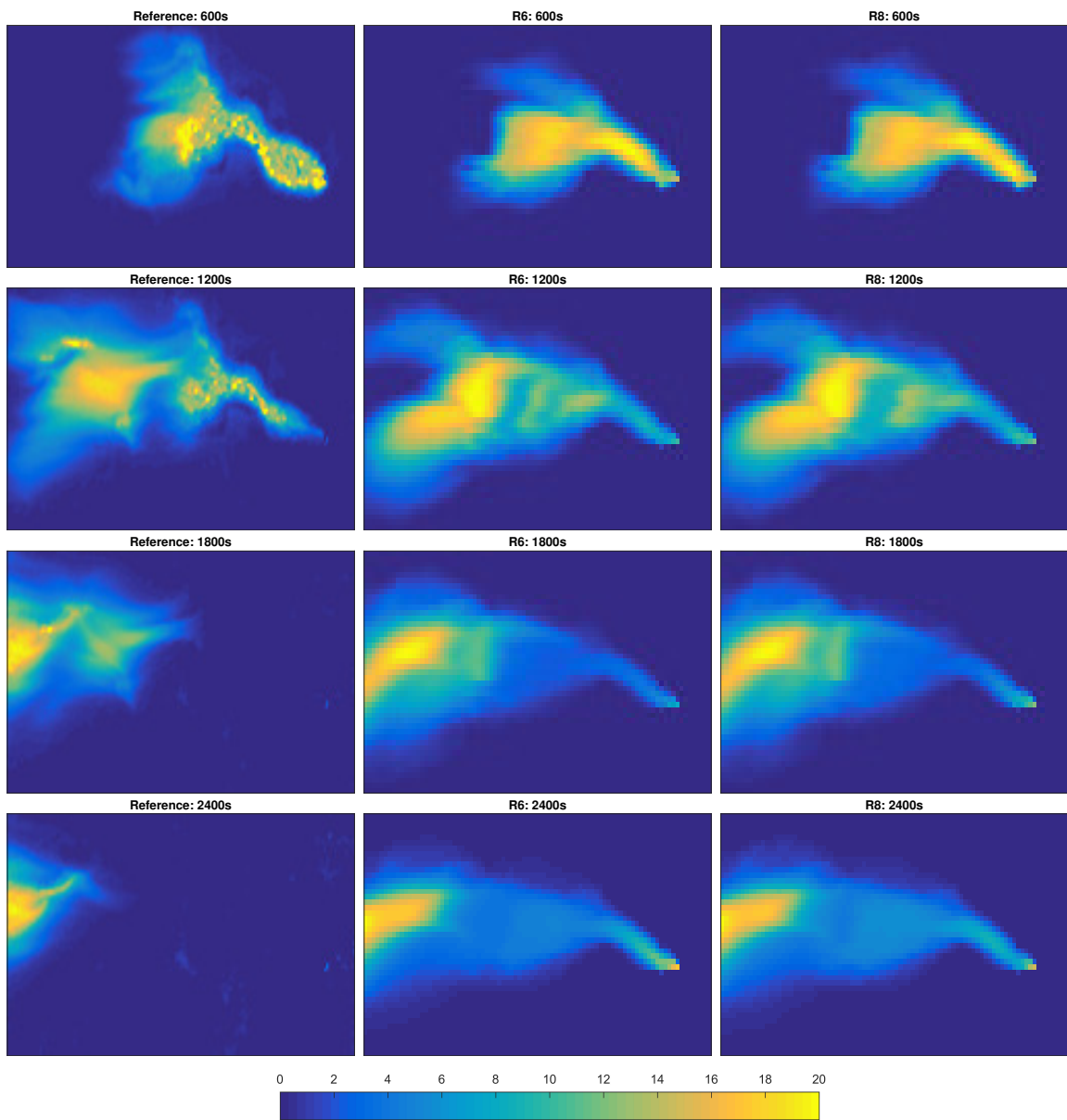


Figure 13: Second sandbox experiment: two pulses. Ensemble mean of the contaminant plume evolution obtained with the updated release functions for scenarios R2 and R4 at 600 s, 1200 s, 1800 s and 2400 s. The first column corresponds to the reference contaminant plume.

328 4. Summary and Conclusions

329 In this paper, we employ the ES-MDA to identify a time-varying release history with
330 different precision in both synthetic and laboratory cases. In the synthetic cases, we examined
331 the capacity of the ES-MDA to identify the release function for (i) different levels of time
332 discretizations, with a ratio of 1 to 6 between the coarsest and finest discretizations; (ii) the
333 impact of the observation data frequency (every other time step versus one step every ten time
334 steps); (iii) the choice of the inflation factors (between Rafiee’s and Evensen’s proposals);
335 and (iv) the impact of the number of iterations in the ES-MDA formulation (between four
336 and eight). In total, 24 scenarios with combinations of the aforementioned features were
337 generated and compared. The results show that the ES-MDA with Rafiee’s scheme has
338 a better performance in most scenarios in our case. Also, in all scenarios, increasing the
339 observation data frequency always improves the identification of the recovered release history
340 curve. The number of iterations, whether four or eight, does not have an important effect on
341 the performance of the ES-MDA. In general, the ES-MDA performs well in recovering the
342 release history, when the discretization is equal to 50 or 100 time steps but displays large
343 fluctuations in the scenarios with 300 time steps. We believe this problem could be alleviated
344 by choosing a different parameterization of the release curve, rather than using uncorrelated
345 uniform random numbers to generate the initial ensemble of realizations.

346 Then, we apply the ES-MDA (using Rafiee’s inflation scheme and eight iterations) to two
347 sandbox experiments using different release history curves, a train of four pulses, and two
348 pulses during the first half of the experiment. The results show that the ES-MDA works
349 well for the train of pulses, but overestimates the injection concentrations for the second
350 experiment after the two pulses have ended. We believe that this poor behavior could be
351 explained again by the parameterization of the injection curves and the magnitude of the
352 concentration observation errors.

353 In conclusion, the ES-MDA is a method capable to identify a time-varying release history

354 in both synthetic and real cases. Better results than the ones presented here could have been
355 obtained with a more elaborated parameterization of the time functions to be identified.

356 5. Acknowledgments

357 Financial support to carry out this work was received from grants PID2019-109131RB-I00
358 and PRX17/00150 funded by MCIN/AEI/10.13039/501100011033. Teng Xu also acknowl-
359 edges the financial support from the Fundamental Research Funds for the Central Uni-
360 versities (B200201015) and Jiangsu Specially-Appointed Professor Program (B19052). The
361 authors would like to thank University of Parma for providing the experimental equipment.
362 Part of the work was performed during a stay of the third author at the University of Parma
363 under the TeachInParma initiative, co-funded by Fondazione Cariparma and University of
364 Parma.

365 References

- 366 Aanonsen, S. I., Nævdal, G., Oliver, D. S., Reynolds, A. C., & Vallès, B. (2009). The
367 Ensemble Kalman Filter in Reservoir Engineering—a Review. *SPE Journal*, *14*, 393–412.
368 URL: <http://www.onepetro.org/doi/10.2118/117274-PA>. doi:10.2118/117274-PA.
- 369 Atmadja, J., & Bagtzoglou, A. C. (2001). State of the Art Report on Mathe-
370 matical Methods for Groundwater Pollution Source Identification. *Environmental*
371 *Forensics*, *2*, 205–214. URL: [http://www.sciencedirect.com/science/article/pii/](http://www.sciencedirect.com/science/article/pii/S1527592201900552)
372 [S1527592201900552](http://www.sciencedirect.com/science/article/pii/S1527592201900552). doi:<http://dx.doi.org/10.1006/enfo.2001.0055>.
- 373 Bagtzoglou, A. C., & Atmadja, J. (2005). Mathematical Methods for Hydrologic Inversion:
374 The Case of Pollution Source Identification. *Water Pollution*, *5*, 65–96. URL: [http://](http://www.springerlink.com/index/10.1007/b11442)
375 www.springerlink.com/index/10.1007/b11442. doi:10.1007/b11442.

- 376 Bao, J., Li, L., & Redoloza, F. (2020). Coupling ensemble smoother and deep learning with
377 generative adversarial networks to deal with non-Gaussianity in flow and transport data
378 assimilation. *Journal of Hydrology*, *590*, 125443. URL: <https://doi.org/10.1016/j.jhydrol.2020.125443>. doi:10.1016/j.jhydrol.2020.125443.
- 380 Bear, J. (1972). *Dynamics of Fluids in Porous Media*. American Elsevier.
- 381 Bertino, L., Evensen, G., & Wackernagel, H. (2003). Sequential Data Assimilation Tech-
382 niques in Oceanography. *International Statistical Review*, *71*, 223–241. URL: <http://doi.wiley.com/10.1111/j.1751-5823.2003.tb00194.x>. doi:10.1111/j.1751-5823.2003.tb00194.x.
- 385 Butera, I., Tanda, M. G., & Zanini, A. (2013). Simultaneous identification of the pollu-
386 tant release history and the source location in groundwater by means of a geostatistical
387 approach. *Stochastic Environmental Research and Risk Assessment*, *27*, 1269–1280.
388 doi:10.1007/s00477-012-0662-1.
- 389 Capilla, J. E., Gómez-Hernández, J. J., & Sahuquillo, A. (1998). Stochastic simulation
390 of transmissivity fields conditional to both transmissivity and piezometric head data—3.
391 application to the culebra formation at the waste isolation pilot plan (wipp), new mexico,
392 usa. *Journal of Hydrology*, *207*, 254–269.
- 393 Carrera, J., & Neuman, S. P. (1986). Estimation of Aquifer Parameters Under Transient
394 and Steady State Conditions: 1. Maximum Likelihood Method Incorporating Prior Infor-
395 mation. *Water Resources Research*, *22*, 199–210. doi:10.1029/WR022i002p00199.
- 396 Chen, Y., & Zhang, D. (2006). Data assimilation for transient flow in geologic formations
397 via ensemble Kalman filter. *Advances in Water Resources*, *29*, 1107–1122. doi:10.1016/j.advwatres.2005.09.007.

- 399 Chen, Z., Gómez-Hernández, J. J., Xu, T., & Zanini, A. (2018). Joint identification of con-
400 taminant source and aquifer geometry in a sandbox experiment with the restart ensemble
401 Kalman filter. *Journal of Hydrology*, *564*, 1074–1084. doi:10.1016/j.jhydro.2018.07.
402 073.
- 403 Chen, Z., Xu, T., Gómez-Hernández, J. J., & Zanini, A. (2021). Contaminant Spill in a
404 Sandbox with Non-Gaussian Conductivities: Simultaneous Identification by the Restart
405 Normal-Score Ensemble Kalman Filter. *Mathematical Geosciences*, *53*, 1587–1615. URL:
406 <https://doi.org/10.1007/s11004-021-09928-y>. doi:10.1007/s11004-021-09928-y.
- 407 Citarella, D., Cupola, F., Tanda, M. G., & Zanini, A. (2015). Evaluation of dispersivity
408 coefficients by means of a laboratory image analysis. *Journal of Contaminant Hydrology*,
409 *172*, 10–23. URL: <http://dx.doi.org/10.1016/j.jconhyd.2014.11.001>. doi:10.1016/
410 j.jconhyd.2014.11.001.
- 411 Cupola, F., Tanda, M. G., & Zanini, A. (2015). Laboratory sandbox validation of pollutant
412 source location methods. *Stochastic Environmental Research and Risk Assessment*, *29*,
413 169–182. doi:10.1007/s00477-014-0869-4.
- 414 Emerick, A. A., & Reynolds, A. C. (2013). Ensemble smoother with multiple data assim-
415 ilation. *Computers and Geosciences*, *55*, 3–15. URL: [http://dx.doi.org/10.1016/j.](http://dx.doi.org/10.1016/j.cageo.2012.03.011)
416 [cageo.2012.03.011](http://dx.doi.org/10.1016/j.cageo.2012.03.011). doi:10.1016/j.cageo.2012.03.011.
- 417 Evensen, G. (2003). The Ensemble Kalman Filter: Theoretical formulation and practical
418 implementation. *Ocean Dynamics*, *53*, 343–367. doi:10.1007/s10236-003-0036-9.
- 419 Evensen, G. (2004). Sampling strategies and square root analysis schemes for the EnKF.
420 *Ocean Dynamics*, *54*, 539–560. doi:10.1007/s10236-004-0099-2.
- 421 Evensen, G. (2018). Analysis of iterative ensemble smoothers for solving inverse problems.

422 *Computational Geosciences*, 22, 885–908. URL: <http://link.springer.com/10.1007/s10596-018-9731-y>.
423

424 Evensen, G., & van Leeuwen, P. J. (2000). An Ensemble Kalman Smoother for Nonlinear
425 Dynamics. *Monthly Weather Review*, 128, 1852–1867. doi:10.1175/1520-0493(2000)
426 128<1852:aeksfn>2.0.co;2.

427 Feyen, L., Gómez-Hernández, J., Ribeiro Jr, P., Beven, K. J., & De Smedt, F. (2003a). A
428 bayesian approach to stochastic capture zone delineation incorporating tracer arrival times,
429 conductivity measurements, and hydraulic head observations. *Water resources research*,
430 39.

431 Feyen, L., Ribeiro Jr, P., Gomez-Hernandez, J., Beven, K. J., & De Smedt, F. (2003b).
432 Bayesian methodology for stochastic capture zone delineation incorporating transmissivity
433 measurements and hydraulic head observations. *Journal of hydrology*, 271, 156–170.

434 Franssen, H., & Gómez-Hernández, J. (2002). 3d inverse modelling of groundwater flow at
435 a fractured site using a stochastic continuum model with multiple statistical populations.
436 *Stochastic Environmental Research and Risk Assessment*, 16, 155–174.

437 Franssen, H. J., & Kinzelbach, W. (2009). Ensemble Kalman filtering versus sequential
438 self-calibration for inverse modelling of dynamic groundwater flow systems. *Journal of*
439 *Hydrology*, 365, 261–274. URL: <http://dx.doi.org/10.1016/j.jhydrol.2008.11.033>.
440 doi:10.1016/j.jhydrol.2008.11.033.

441 Gómez-Hernández, J., Franssen, H.-J. H., & Sahuquillo, A. (2003). Stochastic conditional
442 inverse modeling of subsurface mass transport: a brief review and the self-calibrating
443 method. *Stochastic Environmental Research and Risk Assessment*, 17, 319–328.

444 Gómez-Hernández, J. J., & Xu, T. (2021). Contaminant source identification in aquifers: A
445 critical view. *Mathematical Geosciences*, (pp. 1–22).

- 446 Houtekamer, P. L., & Mitchell, H. L. (2001). A Sequential Ensemble Kalman Filter for At-
447 mospheric Data Assimilation. URL: [http://journals.ametsoc.org/doi/abs/10.1175/](http://journals.ametsoc.org/doi/abs/10.1175/1520-0493(2001)129<0123:ASEKFF>2.0.CO;2)
448 [1520-0493\(2001\)129<0123:ASEKFF>2.0.CO;2](http://journals.ametsoc.org/doi/abs/10.1175/1520-0493(2001)129<0123:ASEKFF>2.0.CO;2).
449 [doi:10.1175/1520-0493\(2001\)129<0123:ASEKFF>2.0.CO;2](https://doi.org/10.1175/1520-0493(2001)129<0123:ASEKFF>2.0.CO;2). arXiv:0203058.
- 450 Huang, C., Hu, B. X., Li, X., & Ye, M. (2009). Using data assimilation
451 method to calibrate a heterogeneous conductivity field and improve
452 solute transport prediction with an unknown contamination source.
453 *Stochastic Environmental Research and Risk Assessment*, *23*, 1155--1167.
454 [doi:10.1007/s00477-008-0289-4](https://doi.org/10.1007/s00477-008-0289-4).
- 455 Kurtz, W., Hendricks Franssen, H.-J., Kaiser, H.-P., & Vereecken, H. (2014).
456 Joint assimilation of piezometric heads and groundwater temperatures for
457 improved modeling of river-aquifer interactions. *Water Resources Re-*
458 *search*, *50*, 1665--1688. URL: <http://doi.wiley.com/10.1002/2013WR014823>.
459 [doi:10.1002/2013WR014823](https://doi.org/10.1002/2013WR014823).
- 460 Lan, T., Shi, X., Jiang, B., Sun, Y., & Wu, J. (2018). Joint inversion of
461 physical and geochemical parameters in groundwater models by sequential
462 ensemble-based optimal design. *Stochastic Environmental Research and Risk As-*
463 *essment*, *32*, 1919--1937. URL: <https://doi.org/10.1007/s00477-018-1521-5>.
464 [doi:10.1007/s00477-018-1521-5](https://doi.org/10.1007/s00477-018-1521-5).
- 465 Le, D. H., Emerick, A. A., & Reynolds, A. C. (2016). An Adaptive Ensemble
466 Smoother With Multiple Data Assimilation for Assisted History Matching.
467 *SPE Journal*, *21*, 2195--2207. URL: <https://doi.org/10.2118/173214-PA>.
468 [doi:10.2118/173214-PA](https://doi.org/10.2118/173214-PA).
- 469 van Leeuwen, P. J., & Evensen, G. (1996). Data Assimilation and Inverse

470 Methods in Terms of a Probabilistic Formulation. *Monthly Weather Re-*
471 *view*, 124, 2898--2913. URL: [http://journals.ametsoc.org/doi/abs/10.1175/](http://journals.ametsoc.org/doi/abs/10.1175/1520-0493(1996)124<2898:DAAIMI>2.0.CO;2)
472 [1520-0493\(1996\)124<2898:DAAIMI>2.0.CO;2](http://journals.ametsoc.org/doi/abs/10.1175/1520-0493(1996)124<2898:DAAIMI>2.0.CO;2).
473 doi:10.1175/1520-0493(1996)124<2898:DAAIMI>2.0.CO;2.

474 Li, J., Lu, W., Wang, H., & Fan, Y. (2019). Identification of groundwater
475 contamination sources using a statistical algorithm based on an improved
476 Kalman filter and simulation optimization. *Hydrogeology Journal*, 27,
477 2919--2931. URL: <http://link.springer.com/10.1007/s10040-019-02030-y>.
478 doi:10.1007/s10040-019-02030-y.

479 Li, L., Zhou, H., & Gómez-Hernández, J. J. (2011). A comparative study of
480 three-dimensional hydraulic conductivity upscaling at the macro-dispersion
481 experiment (made) site, columbus air force base, mississippi (usa). *Jour-*
482 *nal of Hydrology*, 404, 278--293.

483 Li, L., Zhou, H., Gómez-Hernández, J. J., & Hendricks Franssen, H. J.
484 (2012). Jointly mapping hydraulic conductivity and porosity by
485 assimilating concentration data via ensemble Kalman filter. *Journal of*
486 *Hydrology*, 428-429, 152--169. URL: [http://dx.doi.org/10.1016/j.jhydrol.](http://dx.doi.org/10.1016/j.jhydrol.2012.01.037)
487 [2012.01.037](http://dx.doi.org/10.1016/j.jhydrol.2012.01.037). doi:10.1016/j.jhydrol.2012.01.037.

488 Ma, R., Zheng, C., Zachara, J. M., & Tonkin, M. (2012). Utility of bromide
489 and heat tracers for aquifer characterization affected by highly transient
490 flow conditions. *Water Resources Research*, 48.

491 McDonald, M. G., & Harbaugh, A. W. (1988). *A modular three-dimensional finite-*
492 *difference ground-water flow model* volume 6. US Geological Survey Reston, VA.

493 Michalak, A. M., & Kitanidis, P. K. (2004). Estimation of historical
494 groundwater contaminant distribution using the adjoint state method
495 applied to geostatistical inverse modeling. *Water Resources Research*, 40.
496 doi:10.1029/2004WR003214.

497 Rafiee, J., & Reynolds, A. C. (2017). Theoretical and efficient practical
498 procedures for the generation of inflation factors for ES-MDA. *Inverse Prob-*
499 *lems*, 33. doi:10.1088/1361-6420/aa8cb2.

500 Ranazzi, P. H., & Sampaio, M. A. (2019). Ensemble size investigation in
501 adaptive ES-MDA reservoir history matching. *Journal of the Brazilian Society of*
502 *Mechanical Sciences and Engineering*, 41, 413. URL: [http://link.springer.com/](http://link.springer.com/10.1007/s40430-019-1935-0)
503 [10.1007/s40430-019-1935-0](http://link.springer.com/10.1007/s40430-019-1935-0). doi:10.1007/s40430-019-1935-0.

504 Skaggs, T. H., & Kabala, Z. J. (1994). Recovering the release history of a
505 groundwater contaminant. *Water Resources Research*, 30, 71--79. URL: [http://](http://doi.wiley.com/10.1029/93WR02656)
506 doi.wiley.com/10.1029/93WR02656. doi:10.1029/93WR02656.

507 Sun, A. Y., Painter, S. L., & Wittmeyer, G. W. (2006). A constrained robust
508 least squares approach for contaminant release history identification.
509 *Water Resources Research*, 42, 1--13. doi:10.1029/2005WR004312.

510 Todaro, V., D'Oria, M., Tanda, M. G., & Gómez-Hernández, J. J. (2019).
511 Ensemble smoother with multiple data assimilation for reverse flow
512 routing. *Computers & Geosciences*, . URL: [https://linkinghub.elsevier.](https://linkinghub.elsevier.com/retrieve/pii/S0098300419301992)
513 [com/retrieve/pii/S0098300419301992](https://linkinghub.elsevier.com/retrieve/pii/S0098300419301992). doi:10.1016/j.cageo.2019.06.002.

514 Todaro, V., D'Oria, M., Tanda, M. G., & Gómez-Hernández, J. J. (2021).
515 Ensemble smoother with multiple data assimilation to simultaneously
516 estimate the source location and the release history of a contaminant

517 spill in an aquifer. *Journal of Hydrology*, 598. doi:10.1016/j.jhydrol.2021.
518 126215.

519 Wen, X.-H., Capilla, J. E., Deutsch, C., Gómez-Hernández, J., & Cullick, A.
520 (1999). A program to create permeability fields that honor single-phase
521 flow rate and pressure data. *Computers & Geosciences*, 25, 217--230.

522 Xu, T., & Gómez-Hernández, J. J. (2016). Joint identification of
523 contaminant source location, initial release time, and initial solute
524 concentration in an aquifer via ensemble Kalman filtering. *Water Resources*
525 *Research*, . doi:10.1002/2014WR016618.Received.

526 Xu, T., & Gómez-Hernández, J. J. (2018). Simultaneous identification
527 of a contaminant source and hydraulic conductivity via the restart
528 normal-score ensemble Kalman filter. *Advances in Water Resources*,
529 112, 106--123. URL: <https://doi.org/10.1016/j.advwatres.2017.12.011>.
530 doi:10.1016/j.advwatres.2017.12.011.

531 Xu, T., Gómez-Hernández, J. J., Chen, Z., & Lu, C. (2021). A comparison
532 between ES-MDA and restart EnKF for the purpose of the simultaneous
533 identification of a contaminant source and hydraulic conductivity. *Journal*
534 *of Hydrology*, 595, 125681. URL: [https://doi.org/10.1016/j.jhydrol.2020.](https://doi.org/10.1016/j.jhydrol.2020.125681)
535 125681. doi:10.1016/j.jhydrol.2020.125681.

536 Zanini, A., & Woodbury, A. D. (2016). Contaminant source reconstruction by
537 empirical Bayes and Akaike's Bayesian Information Criterion. *Journal of*
538 *Contaminant Hydrology*, 185-186, 74--86. URL: [http://dx.doi.org/10.1016/j.](http://dx.doi.org/10.1016/j.jconhyd.2016.01.006)
539 [jconhyd.2016.01.006](http://dx.doi.org/10.1016/j.jconhyd.2016.01.006). doi:10.1016/j.jconhyd.2016.01.006.

540 Zheng, C. (2010). *MT3DMS v5.3Supplemental users guide: Tuscaloosa, Ala., University*
541 *of Alabama Department of Geological Sciences*. Technical Report Technical Report
542 to the US Army Engineer Research and Development Center.

543 Zheng, C., & Wang, P. P. (1999). MT3DMS: A Modular Three-Dimensional
544 Multispecies Transport Model, . (p. 219).

545 Zhou, H., Gómez-Hernández, J. J., & Li, L. (2014). Inverse methods in
546 hydrogeology: Evolution and recent trends. *Advances in Water Resources*,
547 *63*, 22--37. URL: <http://dx.doi.org/10.1016/j.advwatres.2013.10.014>.
548 doi:10.1016/j.advwatres.2013.10.014.